DE GRUYTER OPEN

Annealing-induced effects on structural and optical properties of $Cd_{1-x}Zn_xS$ thin films for optoelectronic applications

M. Zakria[1]*, Taj Muhammad Khan[1], Abbas Nasir[2], Arshad Mahmood[1]

[1]Nano-devices Lab, National Institute of Lasers and Optronics (NILOP), P.O. Nilore-45650, Islamabad, Pakistan

[2]Department of Applied Physics, Federal Urdu University of Arts, Sciences and Technology, Islamabad, Pakistan

$Cd_{1-x}Zn_xS$ thin films of variable compositions (x = 0.2, 0.4, 0.6, 0.8) were deposited on glass at room temperature by thermal evaporation process. The prepared samples were annealed at two different temperatures (300 °C, 400 °C) for 1 hour in ambient air. The effects of post-annealing on the structural and optical characteristics were investigated using X-ray diffraction (XRD), spectrophotometry, and Raman spectroscopy (RS) methods. XRD studies suggested that the annealed and as-deposited samples belong to wurtzite structure for all Zn concentrations with a preferential orientation along (002) plane. Spectrophotometry analysis of the samples revealed that the energy band gap decreased with annealing temperature. RS investigated different phonon bands and crystalline phases. Two longitudinal optical phonon modes (1-LO, 2-LO) corresponding to monophase hexagonal structure were observed for all $Cd_{1-x}Zn_xS$ samples. The observed red-shift and anti-symmetrical nature of the 1-LO phonon mode can be associated with annealing, while the overall blue-shift, except for x $\leqslant$ 0.6, was caused by the structural disorders in periodic Cd atomic sub-lattices and broken translational symmetry. The spectroscopic results were strengthened by the XRD studies and their results are consistent.

Keywords: *thin film; $Cd_{1-x}Zn_xS$; annealing; band gap; Raman spectroscopy*

1. Introduction

II – VI compound semiconductors thin films and their alloys have potential applications in various optoelectronics devices [1]. By using these materials for photovoltaic and optoelectronics applications, it is necessary to change the synthesis and growth parameters for tuning and optimizing the structural and optical features. Among these materials, CdS is a direct band gap (E_g = 2.42 eV at room temperature) semiconductor that is extensively used as a window material in $CuInSe_2$, $CuIn_xGa_{1-x}Se_2$, CdTe-based solar cells [2]. In these solar cells, the replacement of CdS with higher band gap $Cd_{1-x}Zn_xS$ films (Table 1) can lead to a decrease in window absorption losses, lattice parameter mismatching and electron affinity difference. This results in an increase in short-circuit current and leads to improving the solar cell efficiency [3–5]. The mixing of different

amounts of CdS and ZnS (ZnS band gap energy, E_g = 3.66 eV) makes a continuous series of solid solutions of $Cd_{1-x}Zn_xS$ (x = 0.0 – 1.0) [5]. The characteristics of $Cd_{1-x}Zn_xS$ thin films lie between CdS and ZnS [6, 7]. $Cd_{1-x}Zn_xS$ ternary alloys lead to a systematic variation in the optical and structural properties by adjusting the (Cd:Zn) ratio in $Cd_{1-x}Zn_xS$ compositions [8]. A thin film of this material is a potential candidate for the fabrication of heterojunction solar cells and optoelectronic devices at low production cost [9, 10]. Advancement in semiconductor thin films growth techniques have made it possible to better control the process parameters and finely tune the material characteristics. Recently, different methodologies have been developed for the synthesis of $Cd_{1-x}Zn_xS$ thin films, including electro-deposition [11], vacuum evaporation method [12], successive ionic layer adsorption and reaction [13], metal-organic vapor phase epitaxy [14] etc. However, we present a very simple technique called the thermal evaporation technique that offers many advantages, like

reproducibility, simple mechanism, high deposition rate and economic viability relative to other sophisticated techniques.

In the last two decades, a lot of scientific works have been done on different aspects of various compositions of $Cd_{1-x}Zn_xS$ thin films [15, 16]. The tuneability of physical properties owing to the incorporation of different Zn amounts in $Cd_{1-x}Zn_xS$ films has already been published in our previous paper [17]. Herein, the aim of this research article is to investigate the effect of post-annealing on structural and optical features by controlling the stoichiometric ratio of Cd:Zn and compare them to our previous as-deposited results. Kumar et al. [12] have reported the transmission and X-ray diffraction (XRD) results for as-deposited films. However, they have not carried out an investigation of annealed films for these four compositions and neither Raman investigations. The modulation of structural and optical properties with thermal annealing has been studied, keeping in view that such familiarity will enable us to synthesize materials more appropriate for the photovoltaic cells and other photonic devices. Our research work also includes a comparison study of red and blue-shift as a function of annealing and Zn content. Annealing causes a red-shift, while Zn addition accounts for the blue-shift in the Raman spectra except for $Cd_{0.2}Zn_{0.8}S$ which has not revealed the red-shift caused by annealing, due to Zn rich $Cd_{1-x}Zn_xS$ films.

2. Experimental

2.1. Samples synthesis

$Cd_{1-x}Zn_xS$ (x = 0.2, 0.4, 0.6, 0.8) thin films were prepared from a homogeneous mixture of electronic grade CdS and ZnS powders. The CdS and ZnS powders of different quantity were mixed mechanically by a pestle and a mortar for 1 hour to prepare uniform compositions. The required thin films of four compositions were deposited onto chemically cleaned glass substrates by a thermal coating system. Before the growth, the substrates were ultrasonically cleaned in a sonicator for half an hour followed by isopropanol for 15 min and lastly dried by an air blower. The material was placed in a molybdenum boat and a current of 120 A was applied to the boat to evaporate the target material. During the deposition, the rotational speed of the substrate holder was 90 rpm, vacuum in the chamber was about 2.66×10^{-3} Pa and the deposition time was 14 min. During the deposition, the thickness of the film was measured by a quartz crystal monitor. All $Cd_{1-x}Zn_xS$ films were deposited under the same experimental conditions. Post-annealing was conducted using a high temperature thermostated furnace. For each composition two samples of $Cd_{1-x}Zn_xS$ films were annealed at two different temperatures 300 °C and 400 °C separately for 1 hour under ambient pressure. A temperature rate of 10 °C/min was applied to raise the temperature up to 300 °C, and 400 °C in order to investigate the annealing behavior.

2.2. Diagnostic techniques

The crystal structure of the samples was studied by a Bruker D-8 X-ray diffractometer using CuKα radiation ($\lambda = 1.5405$ Å). The transmission spectra were analyzed relative to a bare glass wafer in the wavelength of 250 to 1000 nm using a UV-Vis-NIR Hitachi spectrophotometer, model U-4001. The optical phonon bands and crystalline phases were assessed by employing the Raman spectroscopy (model MST-4000A, DONGWOO OPTRON Co., Ltd.). He–Cd laser source of emitting wavelength $\lambda = 442$ nm was used as the excitation source. The collection and detection of signals were taken in a scan mode by an objective lens and an air cooled (-50 °C) charged coupled device (CCD) detector. The Raleigh peak at 442 nm was eliminated by a 442 nm cut-off filter. The Raman spectra were obtained in the range of 200 cm^{-1} to 800 cm^{-1} by a DM320 monochromator and ANDOR DV 401A-BV CCD software.

3. Results and discussion

3.1. X-ray diffraction (XRD) analysis

The crystal structure of annealed and as-deposited thin films was determined from XRD patterns (Fig. 1). The as-deposited films are

apparently pale orange and their yellowness decreases with increasing Zn concentration.
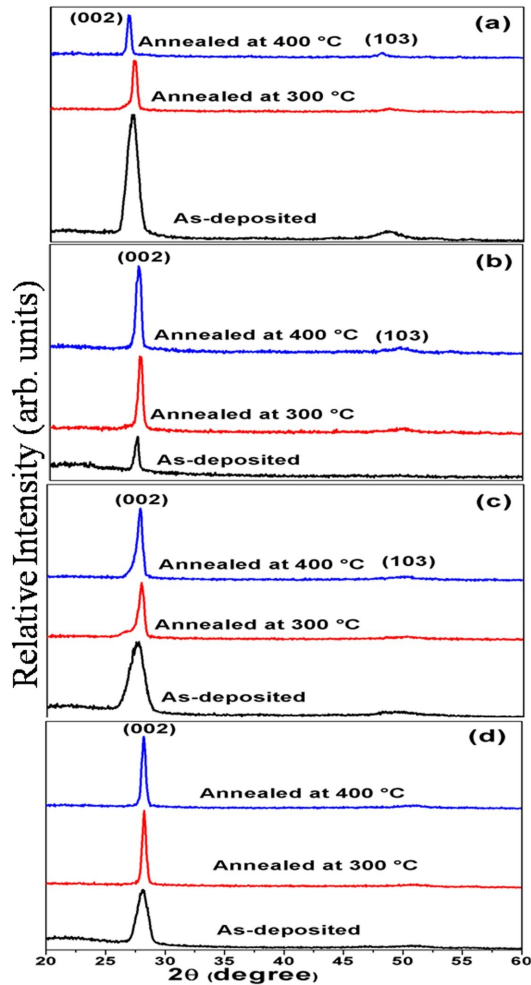

Fig. 1. XRD patterns of the Cd$_{1-x}$Zn$_x$S thin films at various concentrations (a) x = 0.2, (b) x = 0.4, (c) x = 0.6, (d) x = 0.8.

The well-known structural duality characteristics of II – VI compound semiconductors implies that they can be formed either as a cubic zinc blende (sphalerite) or hexagonal (wurtzite) type structures, depending upon the preparation conditions [18]. However, the hexagonal structure is preferable for solar cell applications [12]. It has been investigated from the XRD graph that the as-deposited and annealed samples have polycrystalline nature with the hexagonal crystal structure. The preferred orientation is along (002) plane parallel to the substrate with a very small peak of

(103) plane. The two diffraction peaks of (002) and (103) have been identified and reported by many researchers [19, 20]. It is noteworthy that XRD patterns for the annealed thin films are almost coincident with those of the as-deposited samples. The full width at half maximum peak intensity (FWHM) for the annealed samples decreases with annealing temperature due to grain growth and coalescence of grain boundaries. It is well evident from the XRD patterns that the sharpness of diffraction peaks increases with annealing which reflects the improved crystallinity. There is a marginal variation in peak position in both annealed and as-deposited samples for each composition. The peak angle of (002) plane shifts towards higher angle side with increasing of Zn concentration in the composite film, while the lattice parameters of unit cell decrease, which accounts for the overall tensile strains/stresses developed within the film. The lattice parameters (a and c) of the hexagonal structure can be determined by the following relations [21]:

$$a = \sqrt{\frac{1}{3}} \frac{\lambda}{\sin \theta} \qquad (1)$$

$$c = \frac{\lambda}{\sin \theta} \qquad (2)$$

The crystallite size is estimated from the values of FWHM for the (002) peak in the Debye Scherrer's formula [21]:

$$D = \frac{0.9\lambda}{\beta \cos \theta} \qquad (3)$$

where $\lambda = 1.5406$ Å is the X-ray wavelength, β is the FWHM in radian, θ is half of the peak angle, and D is the crystallite size. All the calculated values for the as-deposited and annealed films are summarized in Table 1.

We have concluded from the structural analyses, that at the annealing temperature of 300 °C, the crystallite size has increased compared to the as-deposited films and remained almost constant at 400 °C except for Cd$_{0.4}$Zn$_{0.6}$S sample which showed a drastic change. In other words, the crystallite size increased with temperature until

Table 1. Prior and post-annealing structural and spectroscopic parameters of $Cd_{1x}Zn_xS$ (x = 0.2, 0.4, 0.6, 0. 8) thin films.

Composition/Temperature		Grain size (nm)	Peak angle [2θ]	FWHM [2θ]	d-spacing [Å]	(h k l)	Band gap [eV]	Lattice constant a[Å]	Lattice constant c [Å]	Physical thickness [nm]
$Cd_{0.8}Zn_{0.2}S$	RT	15.12	26.96	1.08	3.30	(002)	2.51	3.81	6.61	345
	300 °C	46.12	27.05	0.35	3.29		2.42	3.80	6.59	
	400 °C	46.08	26.59	0.35	3.29		2.44	3.87	6.70	
$Cd_{0.6}Zn_{0.4}S$	RT	34.77	27.36	0.47	3.26	(002)	2.69	3.76	6.51	300
	300 °C	38.03	27.60	0.43	3.29		2.47	3.73	6.46	
	400 °C	38.03	27.52	0.43	3.29		2.47	3.74	6.48	
$Cd_{0.4}Zn_{0.6}S$	RT	12.39	27.57	1.32	3.29	(002)	2.74	3.73	6.46	326
	300 °C	37.88	27.89	0.43	3.19		2.64	3.69	6.39	
	400 °C	51.95	27.78	0.31	3.21		2.66	3.70	6.42	
$Cd_{0.2}Zn_{0.8}S$	RT	19.49	28.12	0.84	3.29	(002)	3.10	3.66	6.34	352
	300 °C	34.11	28.18	0.48	3.16		2. 91	3.65	6.33	
	400 °C	34.11	28.13	0.48	3.17		2.91	3.66	6.34	

saturation occurred at 400 °C. The increase in the average crystallite size can be connected to the interface merging process stimulated by annealing treatment. The reactions on the interface can be connected with the existence of interface defects at the crystallite boundaries induced by the annealing treatment owing to random orientation of the crystallites. On the crystallite boundaries, there are several Zn/Cd defects (dangling bonds) and these defects serve as active sites for the merging process, resulting in larger grains or crystallites. This grain growth with temperature shows that crystallinity has improved with annealing. Moreover, the increase in crystallite size with thermal annealing results in reduction of the inter-grain boundaries density, contributing to the decrease in resistivity of the films [22].

3.2. Optical analysis

The transmission spectra of as-deposited and post-annealed samples in the wavelength range of 250 to 1000 nm are shown in Fig. 2.

Transmission spectra of all samples show oscillatory behavior due to thin film interference. Since the amplitude of oscillations relates to the difference in refractive indices of films and substrate, it qualitatively indicates that the film refractive index changes after annealing. The sharp fall of the transmission graph line at the band edge reflects good crystallinity of the films. All the light is absorbed at shorter wavelength regime, whereas for the longer wavelength, electronic transition is decreased, which accounts for the high transmission. A transmission less than 100 % may be due to reflection, scattering and other absorption losses. The optical energy at which absorption starts seems to be fundamental characteristics for each material. Moreover, the effect of annealing is reflected in the decrease in transmittance value with increasing annealing temperature. It could be attributed to light reflection from the rough surface, because the annealing treatment induces grain growth and agglomerations which finally make the surface rough. The linear behavior of the graph at the absorption edge in transmission spectra confirms that the films are direct band gap semiconductors. The interference fringes in transmission spectra become broader after annealing.

To calculate the band gap energy (E_g) of $Cd_{1-x}Zn_xS$ films, we have used Tauc's relation [23]:

$$(\alpha h\nu)^2 = C(h\nu - E_g) \qquad (4)$$

where C is a constant, E_g is the material optical band gap energy and h is Planck's constant. The absorption coefficient α has been found using the
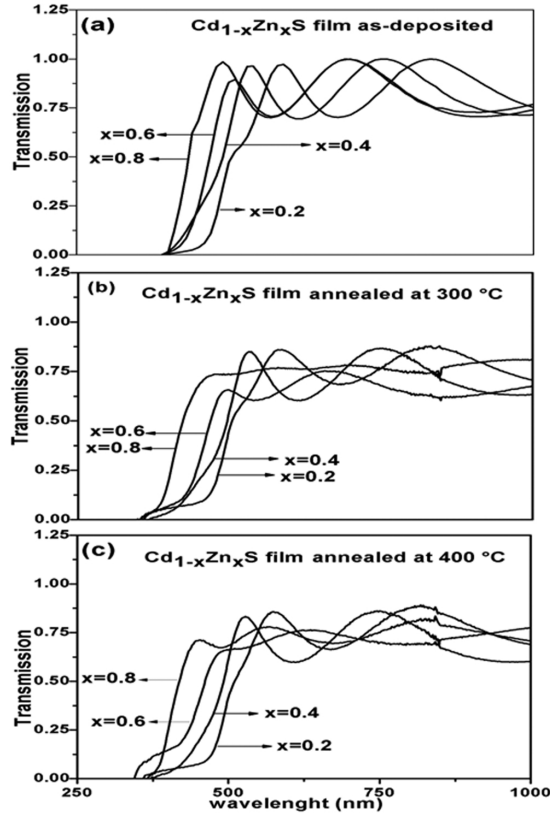
Fig. 2. Transmission spectra of the as-deposited and annealed Cd$_{1-x}$Zn$_x$S thin films with various x.

Fig. 3. The $(\alpha h\upsilon)^2$ vs. $h\upsilon$ plot of (a) as-deposited, and annealed films at (b) 300 °C, (c) 400 °C at various x ratio.

following equation [17]:

$$\alpha = \frac{-\ln T}{t} nm^{-1} \qquad (5)$$

Here, T is the normalized transmittance value at each wavelength, and t is the thickness of film which comes from the quartz crystal monitor measurement during deposition in the vacuum chamber. Fig. 3 shows the relationship between $(\alpha h\upsilon)^2$ and $(h\upsilon)$.

From the model of allowed direct interband transitions, the band gap energy value is obtained by the extrapolation of the linear part of the plot to the $(\alpha h\upsilon)^2 = 0$. The falling edge of the spectral transmittance shifts to longer wavelength side with thermal annealing. By increasing annealing temperature, the grain size increases, while the band gap energy decreases [24]. The band gap energy decrease with annealing may be due to the reduction of quantum size effect, which confirms
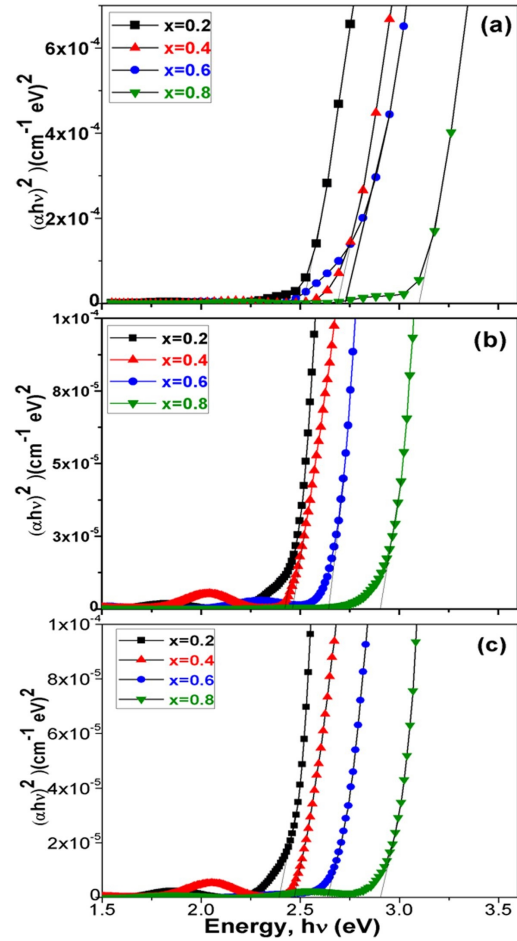
that the size of crystallites in the as-prepared films is small enough to cause the quantum effect [25]. The values of the optical band gap are in close agreement with the values reported by Patidar et al. [5]. Furthermore, the red-shift in the optical band-gap can be better correlated to the crystallite size using the effective-mass approximation [26]. Under this approximation, the size dependence of band gap (E*) can be represented as follows:

$$E^* = E_g + \frac{h^2}{8\mu R^2} - \frac{1.8e^2}{4\pi\varepsilon_o\varepsilon_\alpha R} \qquad (6)$$

where E$_g$ is the material band gap energy, R is crystallite size, μ is the effective mass of the exciton (i.e. hole and electron), ε_o is the material permittivity and ε_α is the high-frequency dielectric con-

stant. The above equation clearly shows that the grain size (R) increases with annealing, while the band gap (E*) decreases and the red-shift occurs. Moreover, the enhancement in optical band gap by the addition of Zn can be described by the nature of ionic bonds present in the crystal lattice. An ionic bond in CdS, can give two Cd^{+2} and S^{-2} ions occupying the lattice sites. Nevertheless, it is obvious for the II – IV compounds crystal structure that there is a significant level of homopolar bonds, while the ionic bond nature also exists in varying degrees due to exchange of electrons. There is an increase in iconicity with the decrease in atomic weight, i.e. from HgTe to ZnS. Therefore, the replacement of Zn with Cd in $Cd_{1-x}Zn_xS$ increases the ionic bonds, which directly results in the lattice strengthening; melting point raising and the increase in band gap [27]. The nature of this optical band gap tuning may be quite useful for a window material for solar cells and other optoelectronic devices.

3.3. Raman spectroscopy analysis

Raman scattering gives information about the crystal structure on the scale of a few lattice constants and is very sensitive to material composition. Raman spectroscopy was carried out with 442 nm excitation wavelength. Fig. 4 shows typical Raman spectra of $Cd_{1-x}Zn_xS$ thin films annealed at temperatures (300 and 400 °C).

From the Raman spectra, it is well evident that the $Cd_{1-x}Zn_xS$ films show two phonon bands so-called longitudinal optical (LO) phonon modes of hexagonal $Cd_{1-x}Zn_xS$ designated as 1-LO, 2-LO and peaked at 307, 315, 316, 327 and 613, 629, 630 cm^{-1}, respectively. These peaks are shifted towards higher Raman shift side in comparison to the 1-LO phonon peak of CdS ($\sim$297 cm^{-1}) [28–30]. A prominent 1-LO phonon mode and a 2-LO second harmonic phonon mode of comparatively less intensity were found for all the compositions and at all temperatures except for the sample with x = 0.8. The designated modes are the 1st and 2nd harmonic overtones of the hexagonally structured $Cd_{1-x}Zn_xS$ thin films. In the Raman spectra, no Raman peak corresponding to the
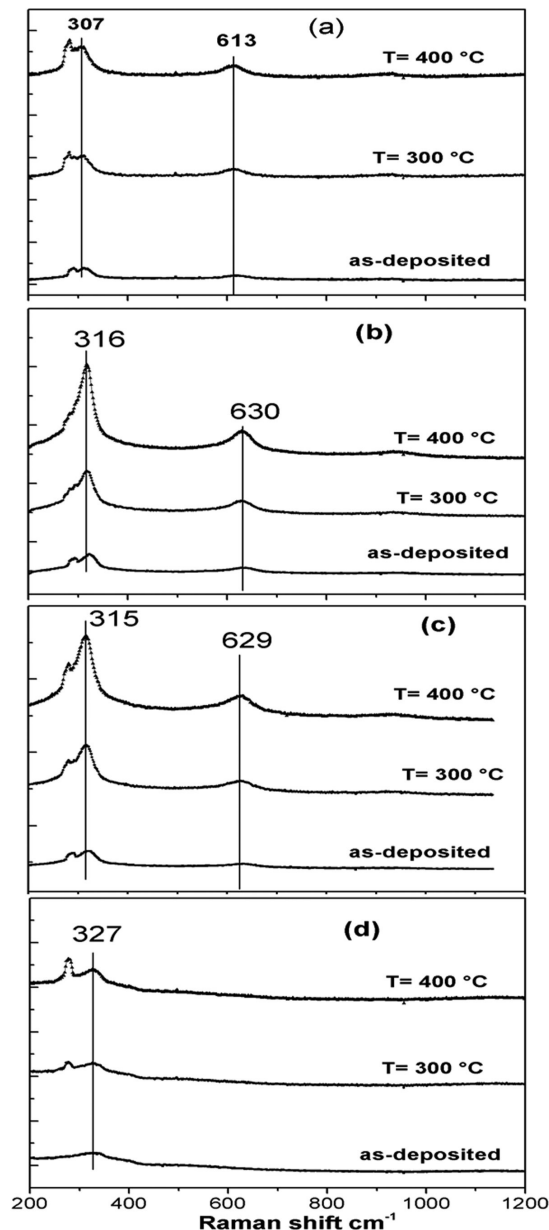

Fig. 4. Raman spectra of the $Cd_{1-x}Zn_xS$ thin films with various compositions (a) x = 0.2, (b) x = 0.4, (c) x = 0.6, (d) x = 0.8.

cubic phase of $Cd_{1-x}Zn_xS$ is observed, which confirms the synthesis of h-$Cd_{1-x}Zn_xS$ thin films, proven by the XRD results. Consequently, our XRD and Raman results support each other. From the figure, it is quite obvious that the 1-LO mode shifts monotonically to lower wave number (red-shift) as a function of annealing temperature for each composition. Such a shift indicates that the

deposited films suffer tensile strain which increases with crystallite size. However, for all the samples a blue-shift occurs for the 1-LO band from 307 to 327 cm^{-1} as Zn concentration increases and presents a broad structure except for the composition with x = 0.6. This accounts for the prominent role of concentration that rules out the annealing effect and induces larger tensile strain within the film than the compressive one. Furthermore, the intensity of 1-LO mode increases with thermal annealing for each composition. Interestingly, the intensity of the 2-LO mode has also increased with annealing, however, for the concentration x = 0.8, this mode does not longer exist and disappears (Fig. 4).

Nevertheless, a phonon band at ~287 cm^{-1} appears as either a kink at the shoulder or as a separate peak on the lower wave number side as the LO phonon which represents the system peak as it lies within the width of this phonon and cannot be assigned to as the sample peak. For all the samples, the 1-LO peak has anti-symmetric nature. To explain and more clearly understand the anti-symmetric nature of the 1-LO phonon mode, it can be related to the presence of defects and disorder in the crystalline structure of the films induced by the Zn atoms impurity in the Cd crystal host lattice. Moreover, Zn substitution in the CdS lattice randomly produced microscopic structural and topological disorders in the periodic Cd atomic sublattice and broke translational symmetry, thus, leading to potential fluctuation and asymmetric broadening [31, 32].

4. Conclusions and outlook

We studied the post-annealing effects of thermally evaporated Cd$_{1-x}$Zn$_x$S films deposited at room temperature. These films were purely monophase, polycrystalline in nature with hexagonal structure. The crystalline structure and film quality improved with thermal annealing. From transmission spectra, the interference fringes became wider after annealing. The post-annealed energy band gap decreased, while an increasing tendency appeared with the addition of Zn.

Raman spectroscopy study revealed that the post annealing produced tensile strain in the films as indicated by the red-shift in 1-LO bands. The annealing induced tensile strain caused also a decrease in the band gap. Our investigations on the modulation of the optical and structural characteristics of the room temperature Cd$_{1-x}$Zn$_x$S thin films with annealing would lead to fabrication of promising materials for the solar cells and other optoelectronic applications.

References

[1] GUTOWSKI J., HEINKE H., HOMMEL D., MICHLER P., *Phys. Status Solidi B*, 229 (2002), 1.
[2] MORKEL M., *Appl. Phys. Lett.*, 79 (2001), 4482.
[3] YAMAGUCHI T., MATSUFUSA J., YOSHIDA A., *Jpn. J. Appl. Phys.*, 31 (1992), 703.
[4] BEDIR M., KAYALI R., OZTAS M., *Turk J. Phys.*, 26 (2002), 121.
[5] PATIDAR D., SAXENA N.S., SHARMA T.P., *J. Mod. Opt.*, 55 (2008), 79.
[6] YOKOGAWA T., ISHIKAWA T., MERZ J.L., TAGUCHI T., *J. Appl. Phys.*, 75 (1994), 2189.
[7] CHU T.L., CHU S.S., BRITT J., FEREKIDES C., WU C.Q., *J. Appl. Phys.*, 70 (1991) 2688.
[8] YAMAGUCHI T., YAMAMOTO Y., TANAKA T., DEMIZU Y., YOSHIBA A., *Thin Solid Films*, 281 – 282 (1996), 375.
[9] DZHAFAROV T. D., ONGUL F., KARABAY I., *J. Phys. D Appl. Phys.*, 39 (2006), 3221.
[10] TORRES J., GORDILLO G., *Thin Solid Films*, 207 (1992), 231.
[11] ASHOKKUMAR M., MUTHUKUMARAN S., *Phys. Procedia*, 49 (2013), 137.
[12] KUMAR P., MISRA A., KUMAR D., DHAMA N., SHARMA T.P., DIXIT P.N., *Opt. Mater.*, 27 (2004), 261.
[13] LAUKAITLSH G., LINDROOS S., TAMULEVICIUS S., LESKELA M., RACKAITIS M., *Appl. Surf. Sci.*, 161 (2000), 396.
[14] YAMAGA S., YOSHIKAWA A., KASAI H., *J. Cryst. Growth*, 99 (1990), 432.
[15] RAJATHI S., SANKARA SUBRAMANIAN N., RAMANATHAN K., SENTHAMIZHSELVI M., *Adv. Mat. Res.*, 699 (2013), 606.
[16] TIAN C., GAO J., LI W., FENG L., ZHANG J., WU L., *Int. J. Photoenergy*, 2012 (2012), ID 549382.
[17] ZAKRIA M., ARSHAD M., SHAH A., RAZA Q., KHAN T.M., AHMED E., *Prog. Nat. Sci.*, 22 (2012), 281.

[18] Bouroushian M., Loizos Z., Spyrellis N., Maurin G., *Appl. Surf. Sci.*, 115 (1997), 103.

[19] Lee J.-H., Song W.-C., Yi J.-S., Yang K.-J., Han W.-D., Hwang J., *Thin Solid Films*, 431 – 432 (2003), 349.

[20] Chavhan S.D., Senthilarasu S., Lee S.-H., *Appl. Surf. Sci.*, 254 (2008), 4539.

[21] Suryanarayana C., Norton M.G., *X-ray Diffraction: A Practical Approach*, Plenum Publishing Corporation, New York, 1998.

[22] Stolyarova S., Weinstein M., Nemirovsky Y., *J. Cryst. Growth*, 310 (2008), 1674.

[23] Borse S.V., Chavhan S.D., Sharma R., *J. Alloy. Compd.*, 436 (2007), 407.

[24] Ezema F.I., Ekwealor A.B.C., Osuji R.U., *Turk J. Phys.*, 30 (2006), 157.

[25] Gaewdang N., Gaewdang T., *Mater. Lett.*, 59 (2005), 3577.

[26] Basit S., Akbari H., Zynali H., Shafie M., *Dig. J. Nanomate. Bio.*, 6 (2011), 709.

[27] Bacaksiz E., Cevik U., *Chem. Phys. Lett.*, 427 (2006), 132.

[28] Sethi R., Kumar L., Sharma P.K., Pandey A.C., *Nanoscale Res. Lett.*, 5 (2009), 96.

[29] Mishra S., Ingale A., Roy U.N., Gupta A., *Thin Solid Films*, 516 (2007), 91.

[30] Sahoo S., Dhara S., Sivasubramanian V., Kalavathi S., Arora A.K., *J. Raman Spectrosc.*, 40 (2009), 1050.

[31] Ingale A., Rustagi K.C., *Phys. Rev. B*, 58 (1998), 7197.

[32] Wang J.B., Zhong H.M., Li Z.F., Lu W., *J. Appl. Phys.*, 97 (2005), 086105.